ORIGINAL PAPER

Isolation of chitosan from shrimp shell (*Metapenaeus monoceros*) as adsorbent for removal of metanil yellow dyes

Putri Ramadhani[1] · Zulkarnain Chaidir[2] · Zilfa Zilfa[3] · Syiffa Fauzia[1] · Rahmiana Zein[1]

Abstract

In this present study, chitosan derived from shrimp shells has been successfully extracted and employed as an adsorbent for metanil yellow dyes using the batch method. The yield of obtained chitosan was calculated as 75.22%, water content 8.9%, with %DD 66.81% based on the Baxter baseline method. The adsorption process indicated that the obtained chitosan reached optimum conditions at pH 4, initial concentration 1000 mg L^{-1}, contact time 60 min, adsorbent heating temperature 120 °C, adsorbent dosage 5 g L^{-1}, and particle size 25 μm with adsorption capacity 199.98 mg g^{-1}. The isotherm and kinetics studies revealed that the adsorption of metanil yellow onto chitosan was fitted to the Langmuir isotherm model and followed the pseudo-second-order model. The thermodynamic parameters (ΔG, ΔH, ΔS) indicated that the adsorption process was spontaneous and exothermic. The adsorption–desorption cycles revealed that NaOH 0.1 M has better performance as a desorbing agent after five adsorption–desorption cycles. The use of adsorbents derived from fishery solid waste in this system presents a sustainable effluent treatment method. The raw materials are derived from renewable natural product sources and are available in large quantities. This study revealed that the chitosan from shrimp shells has good potential as a low-cost and environmentally friendly adsorbent.

Keywords Adsorption · Biosorbent · Chitosan · Metanil yellow · Shrimp shell

✉ Rahmiana Zein
mimiedison@yahoo.co.id; rzein@sci.unand.ac.id

Putri Ramadhani
putriramadhanikimia11@gmail.com

Zulkarnain Chaidir
zulkarnainchaidir@sci.unand.ac.id

Zilfa Zilfa
zilfa@sci.unand.ac.id

Syiffa Fauzia
syiffafauzia@gmail.com

1 Laboratory of Analytical Environmental Chemistry, Department of Chemistry, Andalas University, Padang 25163, West Sumatera, Indonesia

2 Laboratory of Biochemistry, Department of Chemistry, Andalas University, Padang 25163, West Sumatera, Indonesia

3 Laboratory of Applied Chemistry, Department of Chemistry, Andalas University, Padang 25163, West Sumatera, Indonesia

Introduction

The high population growth has led to an increase in the amount of solid waste in the environment. The solid waste from organic matter usually contained many chemical compounds that could be utilized for further purposes, yet it was not efficiently used. Nowadays, converting solid organic waste into another form adding value to its material has become a concern in scientific development. Moreover, Indonesia, as a maritime country has abundant marine resources and high seafood consumption. Therefore, the high demand for seafood consumption such shrimps, crabs, and clams generating its shell as a waste raises another environmental issue.

The shell of those crustaceans contains chitosan, a renewable polymeric substance with a wide range of applications such as enzyme immobilization, biomedical industries and adsorbents. Chitosan is considered more applicable because it is biodegradable, non-toxic, and high adsorption rate [1]. Previous work has employed commercial chitosan for reactive blue 21 removals with an adsorption capacity of 70.08 mg g^{-1} [2]. However, the utilization of commercial

chitosan for large scale was considered less effective due to the high price of pure chitosan, which might increase production cost. Thus, various studies have investigated the possibility of exploiting crustacean shell waste as a chitosan and chitin resources [3].

Shrimp shell as a fishery by-product contains 20–40% protein, calcium 20–50%, chitin 15–40%, and other elements such as solutes, fats, and astaxanthin. Chitin is a parent polymer for the synthesis of chitosan through the deacetylation mechanism [4]. Chitosan has a reasonably good ability because it is rich-reactive groups such as hydroxyl and amino groups. Amine groups are hydrolyzed in an acidic medium, forming positively charged species that provides electrostatic interaction with anionic dyes [5].

Approximately, 280.000 tons of textile dyes are disposed from industrial waste each year in the worldwide. Most dyes are toxic organic compounds and also difficult to degrade due to azo group existence (–N=N–) in its structure. Besides, it has carcinogenic, teratogenic and mutagenic effects [6]. For example, metanil yellow or acid yellow 36 (C.I. 13,065) is an azo aromatic amine chemical compound with the IUPAC name sodium salt m − [(p-anilinophenyl) azo] benzenesulfonic acid [7]. This anionic dye was applied as shoe polish, lacquer, leather dyes, pigment manufacturing, colored-water fast ink, and textile [8]. Therefore, it was easily found in the wastewater and harmful to the environment even at a low concentration.

In order to remove this organic pollutant, some technologies have been made use of, such as precipitation, filtration, coagulation, electrochemical, degradation, photolysis technologies, and photocatalysis degradation [9–13]. However, each method has its limitations, such as high energy consumption, high-cost, toxic sludge generation, and complicated process. Recently, the adsorption method is quite popular for removing pollutants in wastewater. The adsorption method is preferred because it is simple, has good efficiency, and can produce purified water [14]. Several adsorbents have been reported for wastewater treatment including *Garcinia mangostana* L fruit shell [15] rambutan seeds [16], durian seeds [17], *Annona muricata* L. seeds [18], saw dust [19], lala clam shell [20], fish scales [21], conch shells [22], malt bagasse [23], shrimp shell [24], catappa shell [25, 26], and silica-BSA [27]. The utilization of solid organic waste or adsorbent-derived polysaccharides can be cost-efficient and environmentally friendly, due to its abundance, biodegradable, renewable, capable of making physical and chemical interactions with the adsorbate molecules, and the environment's aesthetic [28].

Several studies have employed either shrimp shell, chitin or chitosan for dye removal (cationic and anionic dye) and found that the efficiency of those rich-functional groups adsorbent was specified by the dye structure as well [29–32]. Gopi et al. [29] who has utilized chitin nano-whisker from

shrimp shell for crystal violet removal explained that the interaction of hydroxyl group from chitin nano-whisker could form hydrogen bond with positively charged nitrogen ion from crystal violet allowed the adsorption process. Moreover, only 50% of shrimp that can be consumed and leave the rest as waste [33].
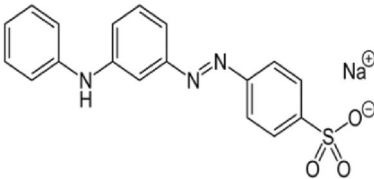
The prior, work which employed the shrimp shell to remove metanil yellow, has an adsorption capacity of 69.30 mg g^{-1} [24]. Due to the low adsorption capacity and to best our knowledge, reports about the use of chitin from shrimp shells to be chitosan through the deacetylation process for wastewater treatment have been reported. Still, research about using chitosan from shrimp shells to the removal of metanil yellow with high adsorption capacity is rarely reported. Therefore, the present study aimed to extract the chitin from shrimp shell to be chitosan and utilized it as an adsorbent to enhance metanil yellow removal in the batch method.

Material and method

Materials and instruments

Shrimp shell (*Metapenaeus monoceros*) as the raw material for chitosan synthesis was obtained from the local area, West Sumatra, Indonesia. Metanil Yellow obtained from Merck, Germany, was used as adsorbate. The chemical structure and its properties are presented in Table 1. Hydrochloric acid 37% (Smart Lab Indonesia company), NaOH p.a (Merck), Etanol p.a (Merck), and deionized water. All reagents were analytical grade. UV–Vis spectrophotometer (Genesys 20 Thermo Scientific, Germany), Fourier transform infrared (FTIR, Unican Mattson Mod 7000 FTIR, USA), scanning electron microscopy–energy-dispersive X-ray (SEM–EDX,

Table 1 Structure and physicochemical of metanil yellow dye

Properties	Dye
Structure	
Molecular formula	$C_{18}H_{14}N_3NaO_3S$
λ_{max}	435 nm
Molecular weight	375.4 g mol^{-1}
Color index	C.I. 13,065
Solubility	25 g L^{-1}
Physical state	Powder
Appearance	Yellow-orange

Hitachi S-3400 N, UK), thermogravimetric analysis (TGA, DTG-60 Simultaneous DTA-TG Apparatus Shimadzu, Japan), and Brunauer, Emmett Teller (BET, Quantachrome Nova 4200e, USA) were use as analytical instruments.

Preparation of raw materials and chitosan extraction

The collected shrimp shells were washed several times with tap water and air-dried. The sample was crushed with a grinder and sieved through a 160-μm sieve. Chitosan from shrimp shell was synthesized by chemical processes, including demineralization, deproteinization, and deacetylation [4]. The demineralization process was carried out by soaking 100 g of sieved shrimp shells in 1 M of HCl (1:10 (w/v)), stirred for 6 h at the room temperature. The mixture was filtered, and the residue was washed until neutral pH was reached. Then, the biosorbent was bleached by soaking in ethanol for 10 min and dried at the temperature of 70 °C. The deproteinization process was done by immersing the demineralized shrimp shell into 1 M NaOH with a ratio of 1:10 (w/v). The function of this process is to extract chitin from shrimp shells. The mixture was stirred for 3 h at 80 °C, filtered, and washed till neutral pH was reached. Then, the biosorbent was bleached according to the procedure above. The deacetylation process was conducted by mixing chitin with NaOH 12.5 M (1:15 (w/v)) stirred for 6 h, and filtered. Then, the residue was washed to remove alkaline excess and dried at 70 °C [4]. The optimum conditions for adsorption of metanil yellow dye were determined using the batch method.

Determination of pHpzc of chitosan

The point of zero charges (pHpzc) was determined by the solid addition method. The analysis was carried out by adding 0.1 g of chitosan to 0.1 M KCl with different pH ranges from 1 to 8 (50 mL each). The suspensions were shaken for 24 h, and the final pH (pHf) of the supernatant was measured. The difference between the initial and final pH, ΔpH (pHf–pHi) was plotted against the initial pH (pHi), and the intersection point resulted from the curve with vertical axis corresponded to the pH point of zero charges (pHpzc) [34].

Adsorption experiments

The effects of pH, initial concentration, contact time, the heating temperature of chitosan, adsorbent dosage, and particle size were investigated on metanil yellow adsorption. The batch method was taken in a 25-mL Erlenmeyer glass flask, by adding a certain amount of chitosan in 10 mL dye solution and stirred at 100 rpm by rotary shaker. After adsorption, the final concentration of metanil yellow dye was determined using a spectrophotometer at 435 nm wavelength. The

adsorption capacity (q, mg g^{-1}) and % removal (%R) were calculated by the following equation:

$$q = \frac{(C_0 - C_e) \times V}{m} \tag{1}$$

$$\%R = \frac{(C_0 - C_e)}{C_0} \times 100 \tag{2}$$

where C_0 (mg L^{-1}) is initial concentration of dye, C_e (mg L^{-1}) is the concentration of dye solution at equilibrium, V (L) is the volume of solution, and m (g) is the mass adsorbent used.

Adsorption isotherm studies

Several adsorption isotherm models such as Langmuir, Freundlich, Temkin, and Dubinin–Radushkevich were used to execute the experimental data. The following equations represented the mathematical model of those isotherm models:

where q_m is the maximum monolayer adsorption capacity of the adsorbent (mg g^{-1}); K_L is Langmuir adsorption constant (L mg^{-1}); q_e is the adsorption capacity at equilibrium (mg g^{-1}); C_e is the concentration of adsorbate in the solution at equilibrium (mg L^{-1}); K_f and n are Freundlich constants; T is the absolute temperature (K); b is Temkin isotherm constant; R is the universal gas constant (8.314 J mol^{-1}); K_T is a constant related to the Temkin isotherm constant (L mg^{-1}); and β is Temkin constant related to the heat of adsorption (J mol^{-1}). In addition, K_{DR} is a constant related to the mean free energy of adsorption (mol^2 J^{-1}); ε is the polyani potential (J mol^{-1}); E is mean free energy of adsorption (kJ mol^{-1}).

The favorability of the adsorption process was analyzed by calculating the separation factor (R_L) expressed by following Eq. (4). The adsorption process was unfavorable, if $R_L > 1$. When $0 < R_L < 1$, the adsorption process was favorable, and the adsorption process was linear if $R_L = 1$, while if $R_L = 0$, the adsorption process was irreversible [35].

Adsorption kinetics studies

To investigate the adsorption kinetics of metanil yellow onto chitosan, the pseudo-first order and pseudo-second order were used to analyze the experimental data. Linear forms of pseudo-first order and pseudo-second order are given in Eqs. (11) and (12):Pseudo-first order:

$$-\ln(q_e - q_t) = k_1 \cdot t - \ln q_e \tag{11}$$

Pseudo-second order:

$$\frac{t}{q_t} = \frac{1}{k_2 q_e^2} + \frac{t}{q_e} \qquad (12)$$

where t is the time (min); q_e is adsorption capacity when equilibrium (mg g^{-1}); q_t is adsorption capacity at a certain time (mg g^{-1}); k_1 and k_2 is pseudo-first-order and pseudo-second-order reaction rate constant (min^{-1}), respectively (Table 2).

Table 2 The mathematical equations of isotherm models

Isotherm models	Equations	
Langmuir	$\frac{1}{q_e} = \frac{1}{k_L q_m C_e} + \frac{1}{q_m}$	(3)
	$R_L = \frac{1}{1+(K_L \times C_0)}$	(4)
Freundlich	$\log q_e = \log K_f + \frac{1}{n} \log C_e$	(5)
Temkin	$q_e = \beta \ln K_T + \beta \ln C_e$	(6)
	$\beta = \frac{RT}{b}$	(7)
Dubinin–Radushkevich	$\ln q_e = \ln q_m - K_{DR} \varepsilon^2$	(8)
	$\varepsilon = RT \ln \left(\frac{C_e + 1}{C_e} \right)$	(9)
	$E = \frac{1}{\sqrt{2K_{DR}}}$	(10)

Fig. 1 Deacetylation process of chitin

Result and discussion

Characterization of biosorbent

The main component for chitosan production is chitin in shrimp shells. Chitin naturally forms the outermost protective layer in shrimp shells by forming a covalent bond with protein, minerals, and carotenoids. The demineralization stage used HCl 1 M to dissolve minerals (generally carbonate and phosphate). Minerals dissolved in acids were indicated by the formation of CO_2 (effervescent) bubbles. The reaction in the demineralization process can be seen in Eq. (13). The deproteinization stage was performed using a low concentration base (NaOH 1 M) to dissolve the protein attached to chitin. An indicator of protein dissolution was a reddish-viscous solution that indicated the formation of sodium proteinate. The deacetylation stage was a hydrolysis reaction of chitin with concentrated bases (NaOH 12.5 M) [4]. At this stage, the acetyl bond (–COCH$_3$) on the amino group in chitin was broken. When the acetyl group was released, the chitin's amide group will bind to a positively charged hydrogen group, forming a free amine group (–NH$_2$) (Fig. 1). This free amine group played a significant role in the binding process of the anionic adsorbate.
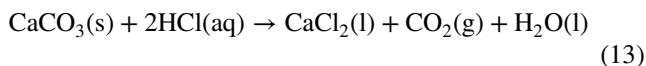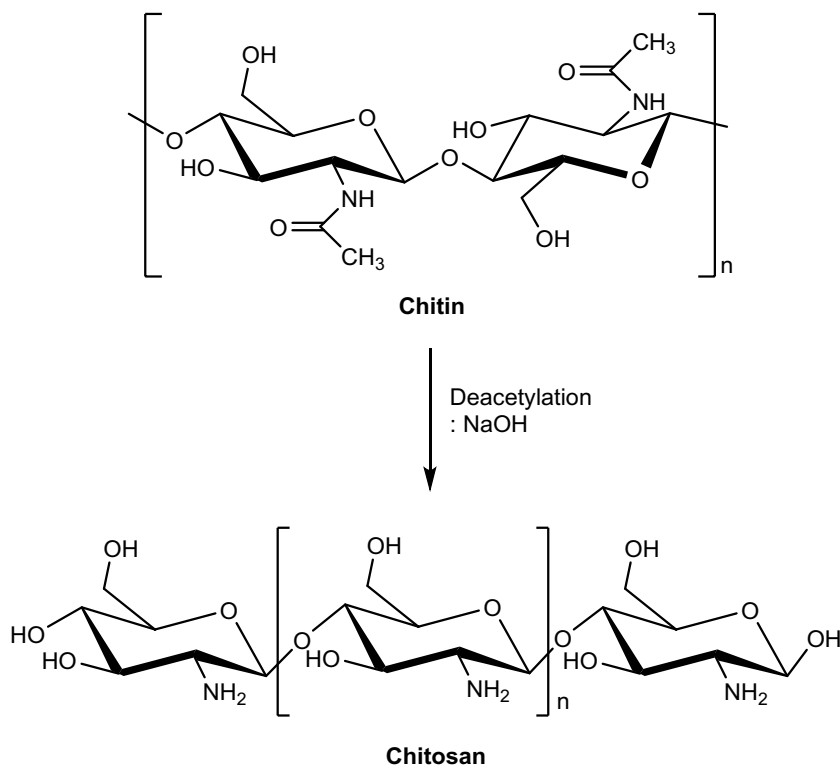
$$CaCO_3(s) + 2HCl(aq) \rightarrow CaCl_2(l) + CO_2(g) + H_2O(l) \qquad (13)$$

The physicochemical characteristics of synthesized chitosan are represented in Table 3.

As shown in Table 3, the percent yield of synthesized chitosan was relatively high. It showed that the synthesis process was adequately effective in producing chitosan from shrimp shells. The moisture content was below the allowed-limit standard ($<10\%$), indicating that obtained chitosan was good. Low water content can extend the storage time of chitosan. The solubility of chitosan was an important parameter because it is related to deacetylation degree, where a high degree of deacetylation showed higher solubility and vice versa [36]. The deacetylation degree was substantial to understand the adsorption capacity of chitosan in metanil yellow removal [31]. In an acidic solution, chitosan with a deacetylation degree (%DD) above 50% was soluble. This was due to the protonation of the amino group on the chitosan. The degree of deacetylation of the synthesized chitosan was 66.81%, which implied that the obtained chitosan contained high amounts of amino groups coming from converting acetyl groups in chitin. The ninhydrin test confirmed the existence of amine groups by turning the color of the solution into purple. DD was determined using FTIR and calculated based on the Baxter baseline method (Eq. 14):

$$\%DD = 100 - \left[\left(\frac{A_{1655}}{A_{3450}}\right) \times 115\right]\% \qquad (14)$$

where A_{1655} is the absorbance at 1655 cm^{-1} of the amide^{-1} band, A_{3450} is the absorbance at 3450 cm^{-1} of the hydroxyl band, and a factor of 155 indicates the A_{3450}/A_{1655} ratio for complete degrees of chitosan deacetylation.

FTIR spectra of chitosan were measured to check the functional group of obtained chitosan before and after the adsorption process (Fig. 2). The chitosan spectrum contained several peaks corresponding to the functional groups that were to bind dye ions. Figure 2 shows a broaden peak at 3000–3600 cm^{-1} was ascribed for the stretching of O–H and N–H bonds. A strong band at 2885 cm^{-1} was attributed to –CH$_2$ in methylene groups that confirmed chitosan existence. The characteristic absorption band at 1600–1700 cm^{-1}

Table 3 Physicochemical characteristics of chitosan from shrimp shell

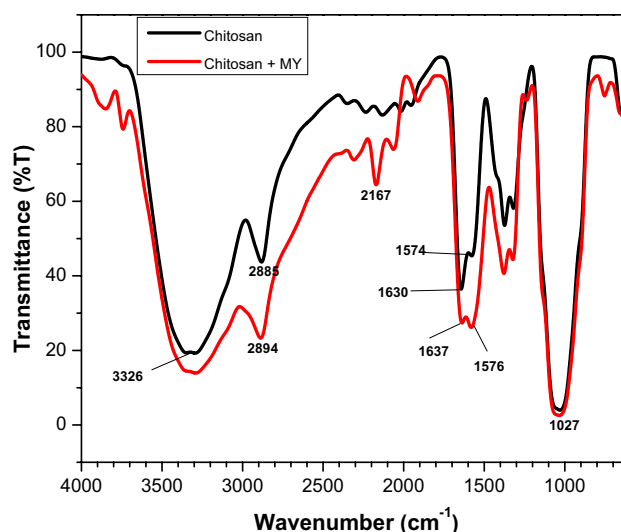| Characteristics	Value
Shrimp shell	100 g
Yield (chitin to chitosan ratio)	75.22%
Form	White powder
Water content	8.9%
Solubility in CH$_3$COOH 2%	Soluble
Ninhydrin test	Forming a purple solution
%DD	66.81%

Fig. 2 FTIR spectra of chitosan before and after adsorption process

represented the stretching vibrations of C=O in amide. The weak peak at 1574 cm^{-1} was assigned to the in-plane N–H bending vibration, a characteristic peak of chitosan polysaccharide. The peak around 1304 cm^{-1} was assigned to C–N vibration. The stretching vibration of C–N or C–O groups represented bands found at 1027 cm^{-1} were characteristic of saccharide structure [4, 37, 38]. After adsorption of metanil yellow, the peak at 2885 cm^{-1}, 1630 cm^{-1}, and 1574 cm^{-1} was shifted to 2894 cm^{-1}, 1637 cm^{-1}, and 1576 cm^{-1}, respectively. However, the difference in wavenumber was not significant. These results suggest the change in the vibrational energy of the functional group. Also, these shifts suggested that the inter- and intra-molecular bond in the chitosan structure has changed due to an interaction between metanil yellow and those functional groups [39]. These results showed that the amine groups were the main functional groups involved in the adsorption of metanil yellow dye.

The surface characteristics of the obtained chitosan before and after the adsorption process were measured by the BET method. As shown in Table 4, the surface area of obtained chitosan was low. This result may be caused by many factors, including the rigid structure found in exoskeletons such as collagen, chitin, chitosan, and

Table 4 Surface characteristic of chitosan before and after metanil yellow adsorption

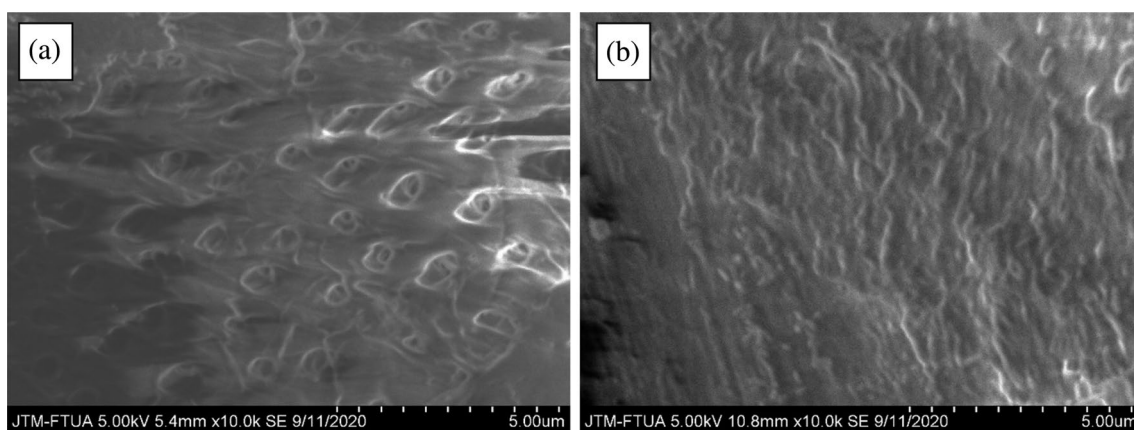| Parameters	Before adsorption	After adsorption
Surface area (m^2 g^{-1})	0.3437	0.3859
Pore volume (cm^3 g^{-1})	0.0029	0.0025
Pore size (nm)	34.6843	26.0189

Fig. 3 SEM image of chitosan: before **a** and after, **b** adsorption

Table 5 EDX analysis of chitosan before and after adsorption

Elements	Before adsorption		After adsorption	
	Weight%	Atomic%	Weight%	Atomic%
C K	62.27	69.19	62.27	69.19
O K	37.23	30.81	37.23	30.81

compounds without the activation process. In addition, the active site's availability was low [40]. As a result, the pore size of obtained chitosan was decreased. On the other hand, the surface area was increased after the adsorption process. This observation proved that the adsorption of metanil yellow onto chitosan has occurred on the surface of the adsorbent. This phenomenon has been verified by the morphology of chitosan measured by the SEM method. The cavities and pores in the chitosan surface (Fig. 3) become smoother after the metanil yellow adsorption process due to the biosorbent surface covering by the homogenous layer of metanil yellow dye. The major elements were carbon and oxygen based on the semiquantitative EDX analysis of the chitosan (Table 5). After the adsorption process, the percentage of oxygen decreased from 37.23 to 33.76%. Meanwhile, the percentage of carbon increased from 62.27 to 66.24%. The increase of carbon percentage probably was originally from carbon in the metanil yellow structure. This percentage indicated that metanil yellow has attached to the surface of chitosan.

The thermogram of obtained chitosan is represented in Fig. 4. It indicated that the initial weight loss (10.25%) was observed between 80 and 150 °C suggesting the vaporization of water molecules due to chitosan dehydration. The second stage of weight loss in the range of 280–430 °C was attributed to the decomposition of chitosan polymer chains. Therefore, it can be concluded that chitosan has low thermal stability. The same result was reported by Kumari et al. [41].
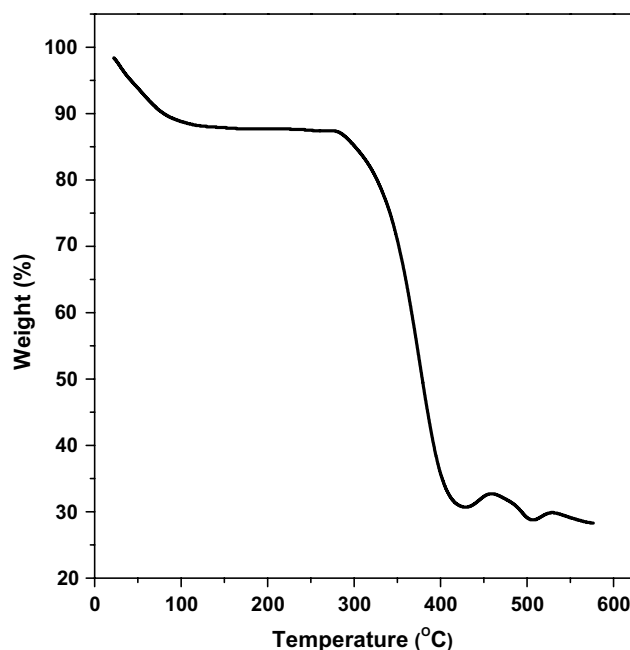

Fig. 4 TGA thermogram of chitosan

pH PZC of chitosan

pHpzc was pH where the surface charge of adsorbent was equal. It meant the number of positive and negative charges on the surface was balanced. The pHpzc provided an important information about sorption mechanisms and indicated the proper pH for adsorbates attached to a particular adsorbent. If solution pH was lower than pHpzc, the positive charge (H^+) on the adsorbent surface increased and was suitable to adsorb the anionic dye due to the increase of electrostatic interaction. In reverse, when the pH adsorbate solution was more significant than pHpzc, the surface contained a large number of negative charge (OH^-), leading to
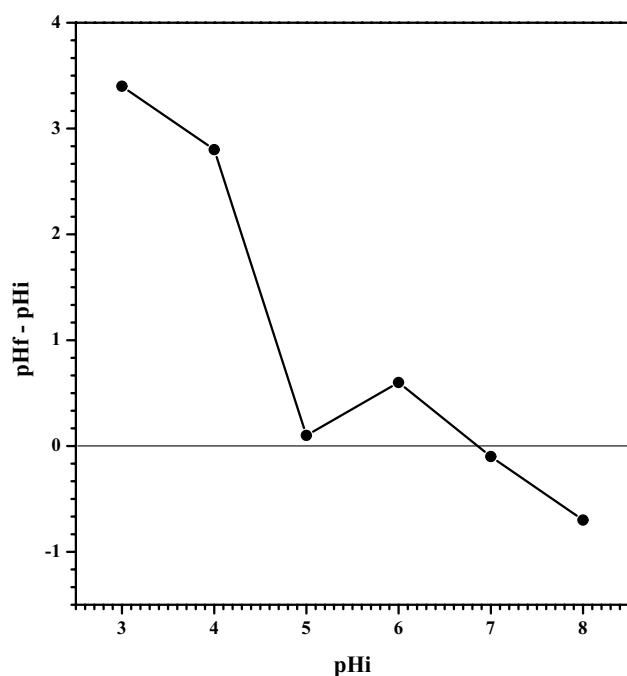
Fig. 5 pHpzc of chitosan

Fig. 6 Effect of pH on adsorption capacity of metanil yellow by chitosan (dye concentration 5 mg L^{-1}, biosorbent dosage 10 g L^{-1}, stirring speed 100 rpm, contact time 60 min, and particle size160 μm)

a repulsion force between adsorbent and anionic dye. Thus, the adsorption capacity decreased.

The pHpzc of obtained chitosan was 6.9 (Fig. 5). In an aqueous solution, the sulfonate groups of metanil yellow dye (D-SO$_3$Na) dissociate became anionic dye ions. Based on this characteristic, it can be predicted that the optimum adsorption of metanil yellow anion will occur at pH < 6.9. The same result has also been reported by Boudouaia et al. [42].

Effect of pH

The initial pH of the dye solution significantly influences the adsorption process because it relates to the dissociation of the dye molecules and the surface charge of the adsorbent. A positive or negative charge in the solution affected the electrostatic interaction between the adsorbent and dye molecule [43].

Figure 6 indicates that the optimum pH of obtained chitosan was 4 with an adsorption capacity of 0.497 mg g^{-1}. The adsorption capacity of the adsorbent decreased as the pH increased. It can be explained that the presence of H$^+$ at low pH facilitated protonation of amino groups of chitosan (R–NH$_2$) forming (–NH^{3+}) ions (Eq. 15). NH$_3^+$ ion will attract to sulfonate group (–SO^{3-}) on the dye molecule, which has undergone dissociation in an aqueous solution (Eq. 16). In this condition, the strong electrostatic attraction between metanil yellow anion and positively charged in chitosan has occurred so that the adsorption capacity increased
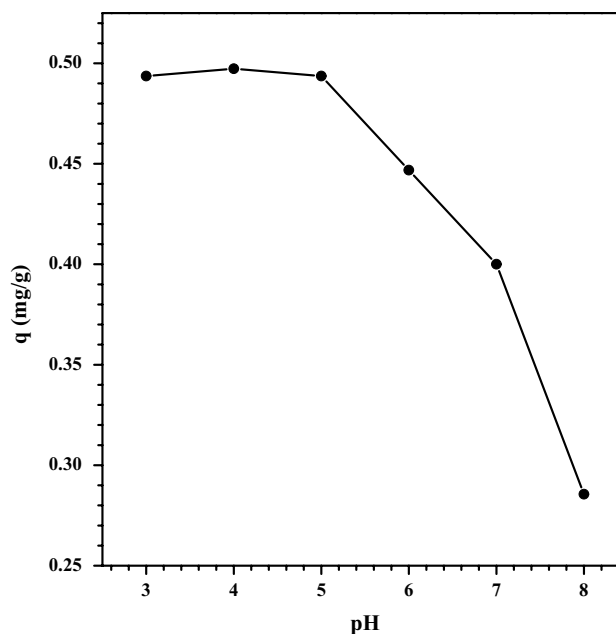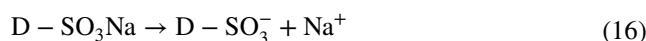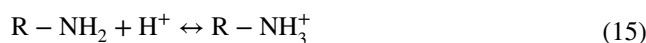
[44]. The possible mechanisms of the adsorption process of metanil yellow by chitosan are represented in Fig. 7.

$$R - NH_2 + H^+ \leftrightarrow R - NH_3^+ \tag{15}$$

$$D - SO_3Na \rightarrow D - SO_3^- + Na^+ \tag{16}$$

The electrostatic interaction between anion of metanil yellow became weaker as pH increased due to the deprotonation of amino groups in alkaline solution. This phenomenon led to electrostatic repulsion between metanil yellow ion and chitosan because the surface charged was negative at the higher pH. For this reason, the adsorption of metanil yellow onto chitosan was low in alkaline pH. The pH optimum for metanil yellow adsorption was obtained at pH < pHpzc (pHpzc = 6.9). The results showed the correspondence between the pHpzc and the effect of pH of solution on the adsorption capacity of chitosan. The same result has been reported by Naghizadeh and Ghafouri [43].

Effect of initial concentration

The initial concentration was related to the driving force of the adsorbate molecules to the active site of the adsorbent. Thus, this parameter affected the interaction of adsorbent and adsorbate in the solution. The effect of the initial concentration of metanil yellow dye was studied in the range of 80–1200 mg L^{-1}.
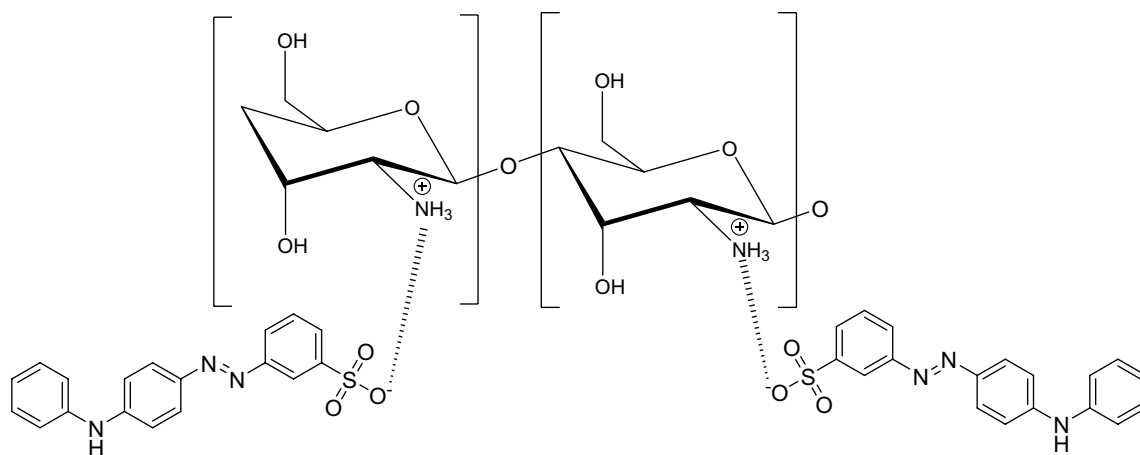
Fig. 7 The possible mechanisms of the adsorption process of metanil yellow by chitosan
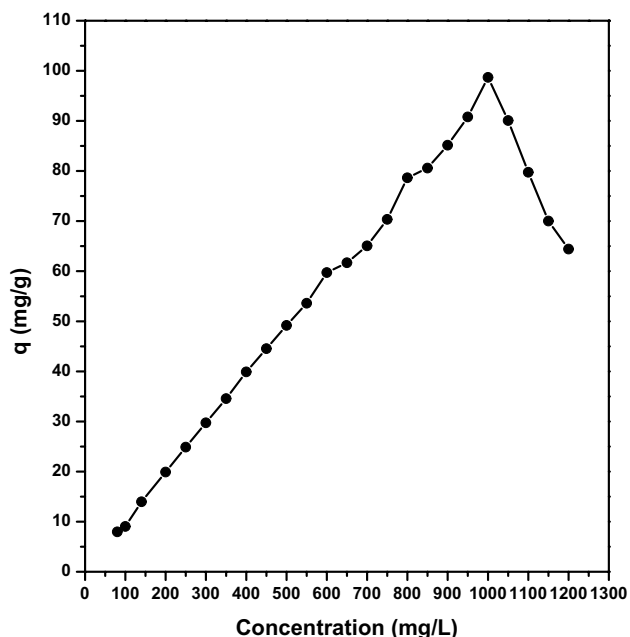

Fig. 8 Effect of initial concentration on adsorption capacity of metanil yellow by chitosan. (pH 4, biosorbent dosage 10 g L^{-1}, stirring speed 100 rpm, contact time 60 min, and particle size 160 μm)

The optimum adsorption capacity was obtained at a concentration of 1000 mg L^{-1} (Fig. 8). Adsorption capacity increased from 7.97 to 98.68 mg g^{-1} within the range of concentration 80–1000 mg L^{-1}, showing that the number of chitosan active sites was sufficient to bind metanil yellow molecules. There was an equilibrium between the number of active sites and metanil yellow molecules at the optimum concentration. The adsorption capacity declined at the higher concentration because the fixed number of active sites can only interact with a certain number of adsorbate, leaving a high concentration of metanil yellow in the solution. It can be concluded that the decrease in adsorption capacity occurred due to the low ratio of adsorbent leading to saturation of active site with high energy level. In case, the adsorption process was initiated from the active site with a low energy level [33, 44, 45].

Effect of contact time

The effect of contact time was essential to describe the adsorption rate and estimated equilibrium time for dye adsorption. The effect of contact time on the sorption of metanil yellow dye was investigated at different time intervals within the range of 15–90 min. The adsorption equilibrium for metanil yellow dye was achieved at 60 min with an adsorption capacity of 98.68 mg g^{-1} (Fig. 9).

The high adsorption rate at the initial stage was due to the availability of functional groups until it reached equilibrium time. As time increased, the number of functional groups decreased because the active sites gradually interacted with the metanil yellow molecule. The adsorption capacity significantly decreased after the optimum condition was achieved since dye molecules were discharged due to the collision during the adsorption process [45, 46]. The same result for the effect of contact time on removing metanil yellow has been reported by Ibrahim and Ibrahim [47].

Effect of biosorbent heating temperature

Heating the adsorbent with a specific temperature range aimed to see adsorbent resistance at the high temperatures. This heating also aimed to reduce the water content trapped in the adsorbent pores so that the surface area became larger.

Figure 10 shows that the adsorption capacity of obtained chitosan significantly decreased at the temperature 210 °C
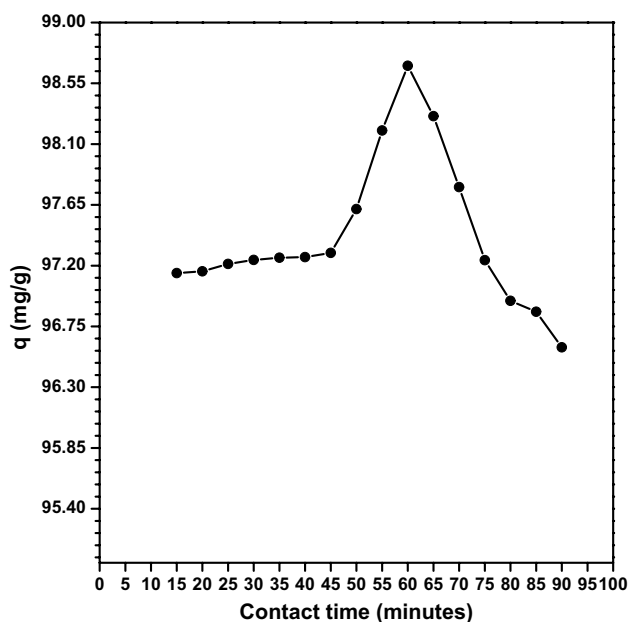
Fig. 9 Effect of contact time on adsorption capacity of metanil yellow by chitosan (pH 4, dye concentration 1000 mg L^{-1}, biosorbent dosage 10 g L^{-1}, stirring speed 100 rpm, and particle size 160 μm)
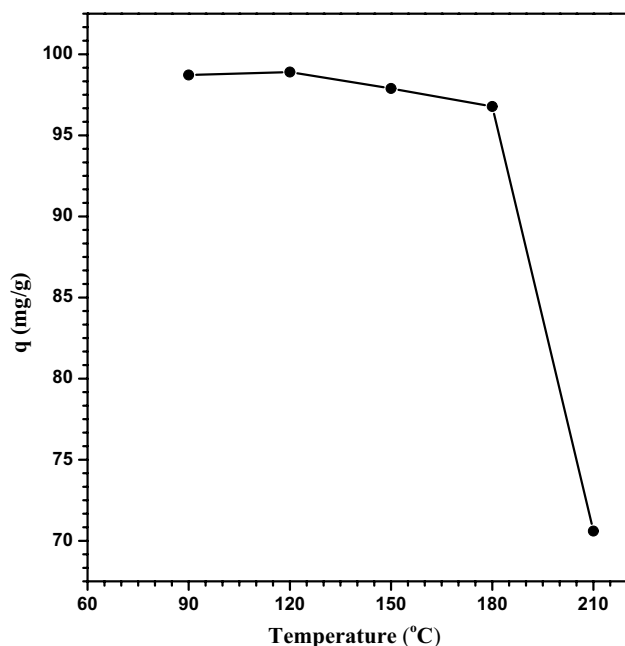

Fig. 10 Effect of temperature on adsorption capacity of metanil yellow by chitosan (pH 4, dye concentration 1000 mg L^{-1}, contact time 60 min, biosorbent dosage 10 g L^{-1}, stirring speed 100 rpm, particle size 160 μm)

and the optimum temperature for the dye metanil yellow adsorption by chitosan occurred at 120 °C with an adsorption capacity of 98.90 mg g^{-1}. This capacity indicated that
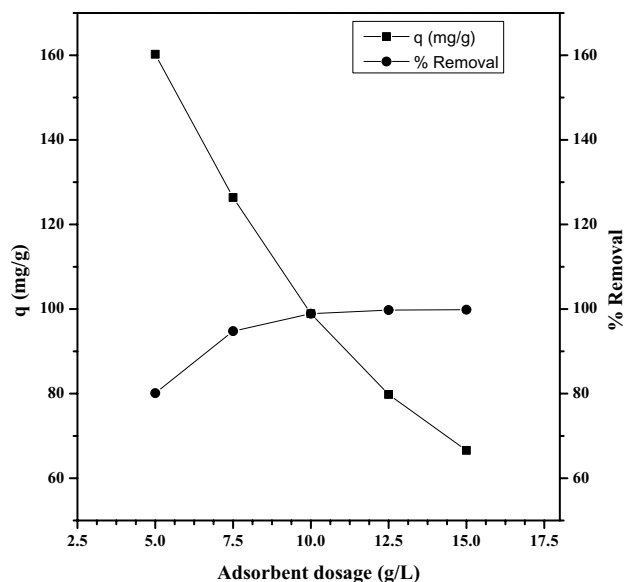

Fig. 11 Effect of adsorbent dosage on adsorption capacity of metanil yellow on chitosan (pH 4, dye concentration 1000 mg L^{-1}, contact time 60 min, stirring speed 100 rpm, heating temperature 120 °C and particle size 160 μm)

the active site and pores were damaged during the heating process, reducing chitosan's ability to interact with the metanil yellow. This phenomenon was confirmed by TGA analysis revealing weight loss of adsorbent due to the heat.

Effect of adsorbent dosage

The effect of adsorbent dosage was related to the adsorbent surface area availability of more adsorption sites and adsorbent–adsorbate equilibrium in the system. This parameter can predict the operating cost per unit of dye solution during the adsorption process [44]. The effect of adsorbent chitosan dosage on metanil yellow removal was studied within range 5; 7.5; 10; 12.5; and 15 g L^{-1}. Figure 11 shows that adsorption capacity decreased as the adsorbent dosage increased. The optimum condition was achieved at adsorbent dosage 5 g L^{-1} with adsorption capacity 160.24 mg g^{-1}. In contra, the % removal of metanil yellow by chitosan increased as adsorbent dosage decreased. The optimum % removal was achieved at adsorbent dosage 15 g L^{-1} with %R 99.85%.

During the adsorption process, the adsorbent's active site was saturated, leading to a decrease in the quantity of dye adsorbed per mass adsorbent. This quantity was related to the surface area reducing of chitosan due to aggregation of adsorbent at the higher dose. Therefore, it can be concluded that at the larger mass of chitosan, the adsorption process may not effectively occur and increase the operating cost [48]. The same result has been reported by Salamat et al. [33].

Effect of particle size

The adsorbent particle size influenced the rate of biosorption directly. The surface area increased by reducing particle size, which increased the number of active sites. Figure 12 shows the effect of particle size of chitosan on metanil yellow dye removal. It can be seen that the adsorption capacity decreased from 199.98 to 137.40 mg g^{-1} as the particle size increased from ≤ 25 to ≤ 425 μm. with the larger particle sizes, the particles' internal layers were inaccessible to adsorbate molecules. The smaller particle sizes made the entire internal layers accessible due to the larger surface area for the adsorption process [48]. It suggested that the smaller the particle size, the adsorption process has occurred optimally. A similar result was reported by Daneshvar et al. [12].

Isotherm studies

The adsorption isotherm was important for determining the adsorption mechanism to explain how adsorbate interrelate with adsorbent materials [49]. The data of adsorption of metanil yellow by chitosan were analyzed using four isotherm models, namely Langmuir, Freundlich, Temkin, and Dubinin–Radushkevich (D–R) isotherms. The linear plots of specific parameters from each isotherm models are shown in Fig. 13. The values of the isotherm model constants were calculated from the slope and intercept of the linear plot
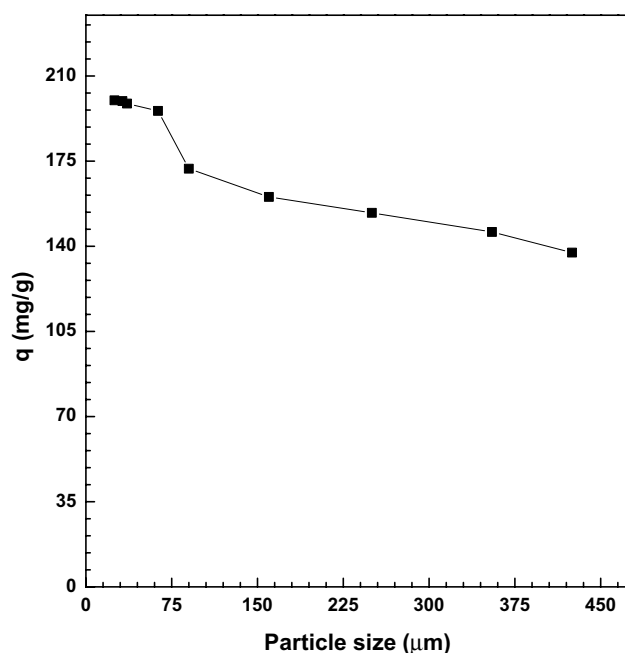
from Langmuir (C_e vs. C_e/Q_e), Freundlich (log C_e vs. log Q_e), Temkin (ln C_e vs. Q_e), and Dubinin–Radushkevich (D–R) (ε^2 vs. ln Q_e). Isotherm model constants were represented in Table 6.

Table 6 summarizes the parameters of each models which were applied. According to the DR model, the average energy of adsorption calculated E was less than 8 kJ mol^{-1}, approving that the adsorption was physical adsorption through the pore on the chitosan surface confirmed by BET and SEM analysis as well [50]. The b values from the Temkin model were related to the heat of adsorption. The high values of b ($b = 260.24$ J mol^{-1}) indicated the sorption process's exothermic and physiochemical nature [51]. Based on R^2 of the Langmuir isotherm model constants was shown excellent linearization and higher R^2 indicated that this model yielded a better fit to the experimental data than other models. These results indicated that chitosan's surface was homogenous and the adsorption process occurred chemically and monolayer sorption process.

The R_L values for chitosan ranged from 0 to 1 according to the Langmuir isotherm results for adsorption of metanil yellow dye, so it can be concluded that the metanil yellow dye adsorption by chitosan was favorable. The Freundlich isotherm supported this adsorption; the values of n were observed to be greater than 1, which suggested that the adsorption process was favorable [35]. The FTIR spectra approved the result of chitosan, where the wavenumber of some functional groups that played a role in the adsorption process has shifted. This phenomenon showed that the interaction between the functional groups and the dye molecule was chemisorption. The same result for RB29 dye adsorption by chitosan was reported by Naghizadeh and Ghafouri [43].

Kinetic studies

One of the criteria for a good adsorbents in wastewater treatment is high adsorption capacity and fast adsorption rate. Thus, it is necessary to analyze the adsorption kinetic to understand those matters. The pseudo-first-order and pseudo-second-order kinetic models were used to obtain the rate constants and equilibrium adsorption capacity. The rate of solution adsorption and residence time for adsorbate at the solution-adsorbent interface can be calculated using these models.

The values of the pseudo-first-order model constants, k_1, and q_e were calculated from the slope and intercept of the plots of t versus ln ($q_e - q_t$) (Fig. 14a). In contrast, the pseudo-second-order model constants, k_2 and q_e were calculated from the slope and intercept of the plots of t versus t/q_t (Fig. 14b). The model parameters determined along with the correlation coefficient values (R^2) are presented in Table 7.
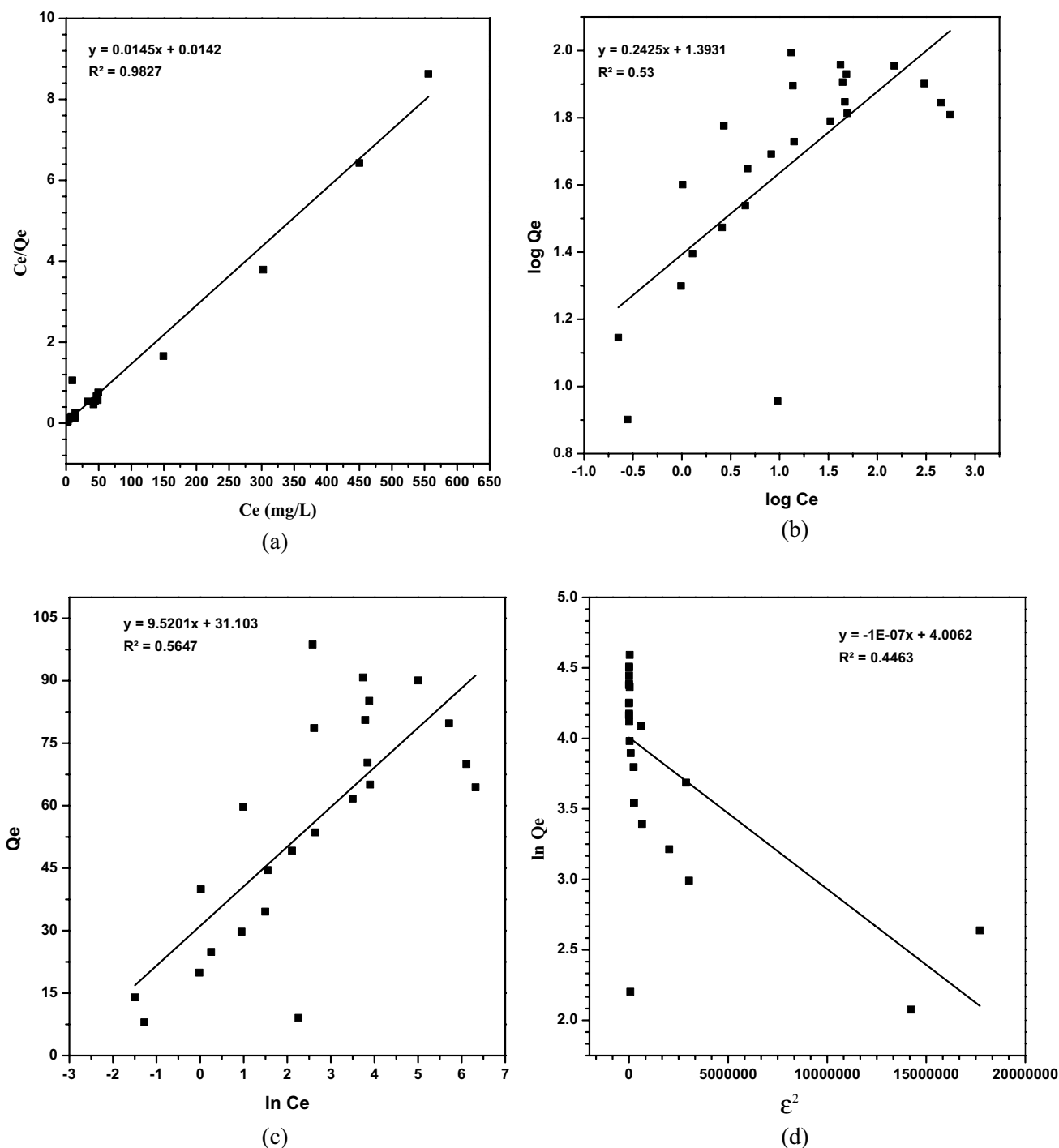

Fig. 12 Effect of particle size on adsorption capacity of metanil yellow on chitosan (pH 4, dye concentration 1000 mg L^{-1}, contact time 60 min, stirring speed 100 rpm, heating temperature 120 °C, and biosorbent dosage 5 g L^{-1})

Fig. 13 Langmuir (**a**), Freundlich (**b**), Temkin (**c**), and Dubinin–Radushkevich (D–R) (**d**) isotherm linear equations for metanil yellow adsorption on chitosan

The low R^2 (< 0.90) value for the pseudo-first-order model, as shown in Table 7, suggests that this model was not sufficient for explain the adsorption kinetic of metanil yellow dye on chitosan. However, for the pseudo-second-order model, the relatively high R^2 (> 0.99) value indicated that the ongoing adsorption mechanism followed pseudo-second-order kinetics.

The calculated qe value (qe_{cal}) showed good agreement with the experimental qe value (qe_{exp}), proving that

Table 6 Coefficients of Langmuir, Freundlich, Temkin, and Dubinin–Radushkevich (D–R) isotherm models for metanil yellow adsorption by chitosan

Langmuir				Freundlich		
q_m (mg g^{-1})	K_L (L mg^{-1})	R^2	R_L	K_F	$1/n$	R^2
70.42	0.96	0.98	0.0008–0.012	24.72	0.24	0.53
D–R				Temkin		
q_m (mg g^{-1})	K_{DR} (mol^2 g^{-1})	E (kJ/mol)	R^2	K_T (L mg^{-1})	b (J mol^{-1})	R^2
54.93	7.02×10^{-15}	1.18×10^{-7}	0.44	26.23	260.24	0.56
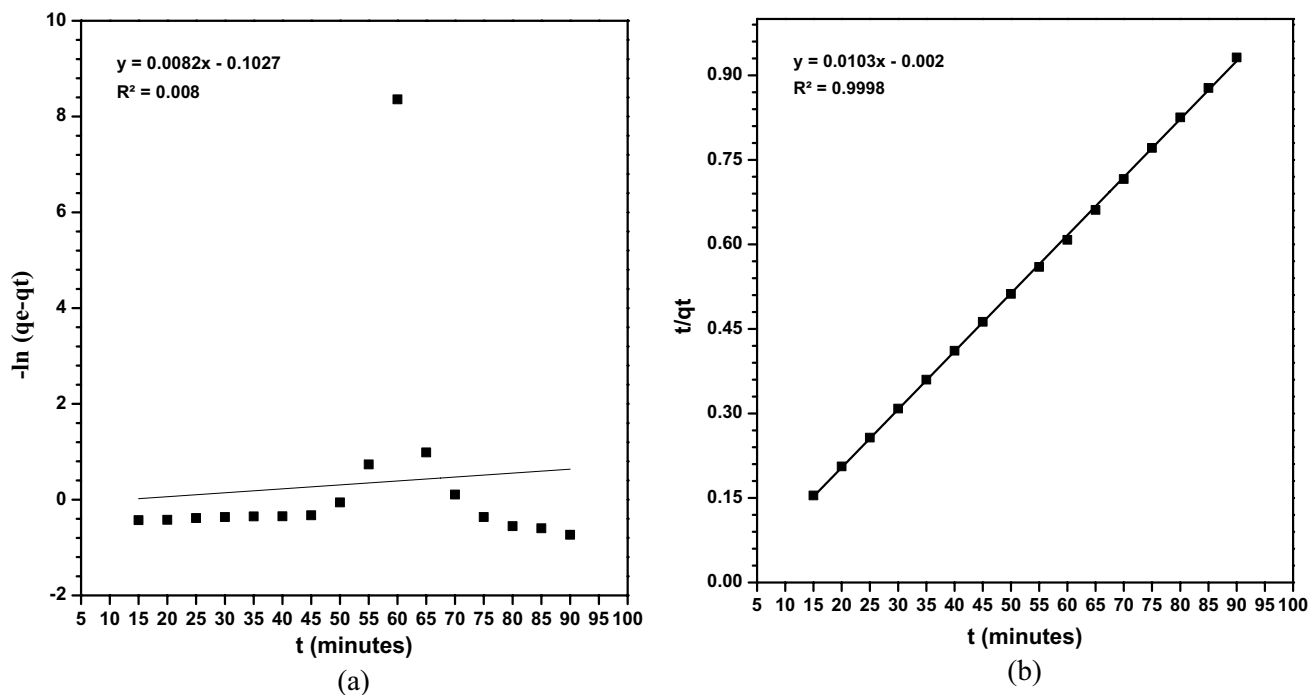
Fig. 14 The curve of adsorption kinetics model **a** pseudo-first order, **b** pseudo-second order of metanil yellow by chitosan

Table 7 The parameter of adsorption kinetics of metanil yellow by chitosan

Pseudo-first order			Pseudo-second order		
K_1 (min^{-1})	Q_e (mg g^{-1})	R^2	K_2 (min^{-1})	Q_e (mg g^{-1})	R^2
0.0082	1.108	0.008	− 0.053	97.08	0.9998

adsorption of metanil yellow onto chitosan was fitted to pseudo-second-order kinetic model. The pseudo-second-order kinetic model's applicability indicated the adsorption process occurred chemically and surface rate-limiting determining step.

Thermodynamic studies

Evaluation of thermodynamic parameters in the adsorption process is important for determining heat change in the system. The thermodynamic parameters, including Gibbs free energy ($\Delta G°$), enthalpy ($\Delta H°$), and entropy ($\Delta S°$), can be calculated at different temperatures and concentrations by using the following equations:

$$\Delta G = -RT \ln(K_L) \tag{17}$$

$$\Delta G = \Delta H - T\Delta S \tag{18}$$

where $R = 8.314$ J mol^{-1} K^{-1} (universal gas constant), K_L (L mol^{-1}) was the equilibrium constant, and T was temperature.

The value of ΔH and ΔS were determined from the slope and intercept, respectively. In order to determine the thermodynamic parameters corresponding to the adsorption of metanil yellow on chitosan, the experiment was carried out at different temperatures (298, 308, and 318 K) and different concentrations (10–50 mg L^{-1}). Thermodynamic parameters of the adsorption metanil yellow onto chitosan are listed in Table 8.

The negative values of ΔG indicate that the adsorption process were viable and spontaneous. The value of ΔG decreased as temperature increased, indicating that the process was more favorable at lower temperatures [52]. The enthalpy change ($\Delta H°$) was negative, indicating the exothermic reaction of the metanil yellow adsorption process. It was also confirmed by the b constant from the Temkin isotherm model. The negative value of ΔS suggested a low-level disorder in the chitosan surface during the adsorption process. This indicated that the initial entropy of dye molecules in the solution was greater than the final entropy in the adsorbent surface, which resulted in the orderliness of the dye molecules at the adsorbent surface [47]. The same result was reported by Boumchita et al. [52].

Adsorption–desorption study

The regeneration is essential to evaluate sorbent repeatability. Therefore, an adsorption–desorption study was conducted to examine the possibility of chitosan and dye regeneration by applying a desorbing agent [53]. The regeneration process was carried out using the batch method and employed NaOH as a desorbing agent. First, the adsorption study was conducted by loaded 10 mL of metanil yellow solution (20 mg L^{-1}, pH 4) with 0.1 g chitosan. The mixture was shaken for an hour at 100 rpm. Then, the desorption study was performed by mixing the dry dye-saturated chitosan from adsorption metanil yellow with 10 mL of NaOH solution (concentration: 0.1 and 0.01 M) [54, 55].

Figure 15 shows that the adsorption capacity was decreased from 1.98 to 1.32 mg g^{-1} after the fifth cycle using NaOH 0.1 M as a desorbing agent. Meanwhile, NaOH 0.01 M as desorbing agent caused a decrease of adsorption capacity from 1.98 to 0.88 mg g^{-1} after the fifth cycle. Therefore, it can be concluded that after five
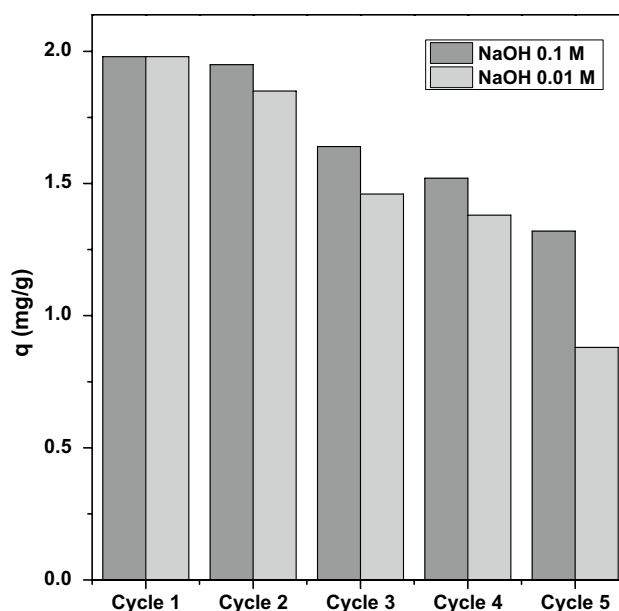

Fig. 15 Adsorption–desorption study of chitosan

times adsorption–desorption cycles, the adsorption capacity did not significantly change. However, a different effect was given by both desorbing agents. Table 9 shows that the higher NaOH concentration gave a higher desorption percentage than the lower NaOH concentration. This phenomenon can be explained that higher base concentration caused an increased number of negative ions (OH$^-$), increasing electrostatic repulsion, which supported the desorption process [56]. The reaction responsible for the desorption of metanil yellow is represented in Eq. 19. The sodium ion from NaOH would be reacted with $D-SO_3^-$ ion from $RNH_3^+D-SO_3^-$ reforming dye molecules itself and released chitosan's functional group (RNH_2) so that it was ready to be employed for the next adsorption–desorption cycles (repeatability).
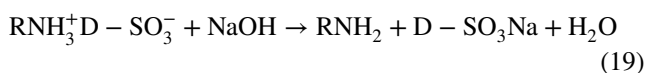
$$RNH_3^+D-SO_3^- + NaOH \rightarrow RNH_2 + D-SO_3Na + H_2O$$
(19)

Table 8 The Thermodynamic parameters of the adsorption metanil yellow onto chitosan

Temperature (K)	ΔG (kJ/mol)	ΔH (kJ/mol)	ΔS (kJ/mol K)
298	− 3346.38	− 50,275	− 156.9
308	− 2294.62		
318	− 208.365		

Table 9 Desorption percentage of metanil yellow using NaOH 0.1 M and 0.01 M

	% Des (NaOH 0.1 M)	% Des (NaOH 0.01 M)
Cycle 1	86.575	81.694
Cycle 2	82.236	68.262
Cycle 3	76.856	50.803
Cycle 4	65.798	35.584
Cycle 5	44.504	16.048

Table 10 Comparison of maximum adsorption capacities of several adsorbent for anionic dye

Adsorbent	Adsorbate	Q (mg g^{-1})	Refs.
Activated carbon from *Gmelina arborea* bark	Metanil yellow	2.35	[57]
Modified carbon sorbent	Metanil yellow	2.31	[58]
Chitosan from Persian gulf shrimp shell	Reactive blue	87.74	[43]
Rice husk	5G blue reactive dye	3.84	[59]
Chitosan functionalized magnetic Nanoparticles	Reactive orange 107	95.23	[37]
Malt bagasse	Yellow Reafix BR2	68.7	[23]
Water hyacinth plant	Metanil yellow	43.5	[60]
Eggshell powder-chitosan gel (EPCG)	Suncion Red H-R (SRH-R) Sunzol Blue RS (SB-RS)	2.794 2.948	[61]
Commercial chitosan	Reactive blue 21	70.08	[2]
Shrimp shell (*Metapenaeus monoceros*)	Metanil yellow	69.30	[24]
Chitosan from shrimp shell (*Metapenaeus monoceros*)	Metanil yellow	199.98	Present study

Table 10 lists the previous work for anionic dyes removal compared to the present study. The differences in adsorption capacity may be affected by the pH of the solution or the degree of the amino group's protonation (for chitosan-based) or the chemical structure and molecular size of the dye or a function of some combination of these factors. The adsorption capacity of chitosan shrimp shell was higher than shrimp shell itself as adsorbent [24]. This indicated that protonated amino groups in the chitosan structure have an important role in metanil yellow removal through electrostatic interaction. Based on the adsorption models and characterization of chitosan, it could be assumed that the adsorption process was controlled by physical-sorption through the pore (based on BET, SEM, and D–R analysis) and dominantly chemical-sorption through electrostatic interaction.

Conclusion

Chitosan from shrimp shell was a good material as an adsorbent to remove metanil yellow dye in wastewater. It was environmentally friendly and low-cost adsorbent. The maximum adsorption capacity was 199.98 mg g^{-1}. The adsorption process followed the isotherm Langmuir models and pseudo-second-order kinetic model. Based on thermodynamic studies, the adsorption process was spontaneous and exothermic in nature. This suggested that the process followed chemisorption through electrostatic interaction. Chitosan derived from shrimp shell as adsorbent showed a significant increase of adsorption capacity rather than shrimp shell itself. This proved that chitosan from shrimp shells could be low-cost, easy generate, and environmentally friendly adsorbent.

References

1. X. Guo, L. Qu, M. Tian, S. Zhu, X. Zhang, X. Tang, K. Sun, Water Environ. Res. **88**, 579 (2016)
2. G. Sreelatha, V. Ageetha, J. Parmar, P. Padmaja, J. Chem. Eng. **56**, 35 (2011)
3. E.H. Abed, N. Imad, A.L. Ameen, L. A. Jazaa **12**, 125 (2017)
4. R.S.C.M. de Q. Antonino, B.R.P.L. Fook, V.A. de O. Lima, R.Í. de F. Rached, N. Lima, Eunice Paloma, R.J. da S. Lima, C.A.P. Covas, M.V.L.F. Fook, Mar. Drugs **15**, 1 (2017)
5. M.B. Kasiri, *Application of Chitosan Derivatives as Promising Adsorbents for Treatment of Textile Wastewater* (Elsevier, Amsterdam, 2019)
6. J. Meng, J. Cui, S. Yu, H. Jiang, C. Zhong, J. Hongshun, R. Soc. Open Sci. **6**, 1 (2019)
7. P.P. Nath, K. Sarkar, P. Tarafder, G. Paul, Int. J. Pharma Bio Sci. **4**, 685 (2013)
8. D. Garg, S. Kumar, K. Sharma, C.B. Majumder, Groundw. Sustain. Dev. **8**, 512 (2019)
9. H. Azizi-Toupkanloo, M. Karimi-Nazarabad, M. Shakeri, M. Eftekhari, Environ. Sci. Pollut. Res. **26**, 30941 (2019)
10. M. Karimi-Nazarabad, E.K. Goharshadi, M. Aziznezhad, ChemistrySelect **4**, 14175 (2019)
11. H. Azizi-Toupkanloo, M. Karimi-Nazarabad, G.R. Amini, A. Darroudi, Sol. Energy **196**, 653 (2020)
12. E. Daneshvar, M.S. Sohrabi, M. Kousha, A. Bhatnagar, B. Aliakbarian, A. Converti, A.C. Norrström, J. Taiwan Inst. Chem. Eng. **45**, 2926 (2014)
13. Zilfa, Rahmayeni, Y. Stiadi, and Adril, Orient. J. Chem. **34**, 887 (2018).
14. G. Xu, Y. Zhu, X. Wang, S. Wang, T. Cheng, R. Ping, J. Cao, K. Lv, E-Polymers **19**, 244 (2019)
15. R. Zein, R. Suhaili, F. Earnestly, Indrawati, and E. Munaf, J. Hazard. Mater. **181**, 52 (2010).

16. R. Zein, A. W. Astuti, D. Wahyuni, F. Furqani, and E. Munaf, Res. J. Pharm. Biol. Chem. Sci. **6**, 86 (2015).

17. Z. Chaidir, R. Zein, D.T. Sagita, E. Munaf, J. Chem. Pharm. Res. **7**, 589 (2015)

18. Z. Chaidir, F. Furqani, R. Zein, E. Munaf, J. Chem. Pharm. Res. **7**, 879 (2015)

19. B. Sushmita, M.C. Chattopadhyaya, Arab. J. Chem. **10**, S1629 (2017)

20. A. Alseddig, A. Eljiedi, and A. Kamari, in *Proceedings of International Conference on Education. Mathematics Science 2016 Conjunction with 4th International Postgraduation Conference Science Mathematics 2016* (2017).

21. F. Marrakchi, M.J. Ahmed, W.A. Khanday, M. Asif, B.H. Hameed, J. Taiwan Inst. Chem. Eng. **71**, 47 (2017)

22. I.E. Ouahabi, R. Slimani, S. Benkaddour, H. Hiyane, N. Rhallabi, B. Cagnon, M. Haddad, S. Antri, S. Lazar, J. Mater. Environme **9**, 1987 (2018)

23. B.C. da Silva, A. Zanutto, J.M.T.A. Pietrobelli, Adsorpt. Sci. Technol. **37**, 236 (2019)

24. P. Ramadhani, Z. Chaidir, Z. Zilfa, Z.B. Tomi, D. Rahmiarti, R. Zein, Desalin. Water Treat. **197**, 413 (2020)

25. L. Hevira, Zilfa, Rahmayeni, O. J. Ighalo, and R. Zein, J. Environ. Chem. Eng. **8**, 104290 (2020).

26. L. Hevira, Zilfa, Rahmayeni, J. O. Ighalo, H. Aziz, and R. Zein, J. Ind. Eng. Chem. **97**, 188 (2021).

27. R. Zein, Z.B. Tomi, S. Fauzia, Z. Zilfa, J. Iran. Chem. Soc. **17**, 2599 (2020)

28. S. Sarode, P. Upadhyay, M.A. Khosa, T. Mak, A. Shakir, S. Song, A. Ullah, Int. J. Biol. Macromol. **121**, 1086 (2019)

29. S. Gopi, A. Pius, S. Thomas, J. Water Process Eng. **14**, 1 (2016)

30. R.G. Sánchez-Duarte, D.I. Sánchez-Machado, J. López-Cervantes, M.A. Correa-Murrieta, Water Sci. Technol. **65**, 618 (2012)

31. A.G.S. Prado, J.D. Torres, E.A. Faria, S.C.L. Dias, J. Colloid Interface Sci. **277**, 43 (2004)

32. M. Fabbricino, L. Pontoni, J. Environ. Chem. Eng. **4**, 4100 (2016)

33. S. Salamat, M. Hadavifar, H. Rezaei, J. Environ. Chem. Eng. **7**, 103328 (2019)

34. M.C. Reddy, L. Sivaramakrishna, A. Reddy, J. Hazard. Mater. **203–204**, 118 (2012)

35. A.A. Inyinbor, F.A. Adekola, G.A. Olatunji, South African J. Chem. **68**, 115 (2015)

36. S. Chawla, S. Kanatt, and A. Sharma, Polysaccharides 1 (2015).

37. T. Saba, F. Minhas, M.I. Malik, F.N. Talpur, A. Jabbar, M.I. Bhanger, Am. J. Anal. Chem. **9**, 633 (2018)

38. S.C. Dey, M. Al-amin, T.U. Rashid, M. Sarker, S. Shamsuddin, Int. J. Latest Res. Eng. Technol. **2**, 52 (2016)

39. J. Ooi, L.Y. Lee, B.Y.Z. Hiew, S. Thangalazhy-Gopakumar, S.S. Lim, S. Gan, Bioresour. Technol. **245**, 656 (2017)

40. G. Niero, A. X. R. Corrêa, G. Trierweiler, A. J. F. Matos, R. Corrêa, H. A. G. Bazani, and C. M. Radetski, AJournal Environ. Sci. Heal. - Part A Toxic/Hazardous Subst. Environ. Eng. **0**, 1 (2019).

41. S. Kumari, S.H. Annamareddy, S. Abanti, P.K. Rath, Afr. J. Biotechnol. **15**, 1258 (2016)

42. N. Boudouaia, Z. Bengharez, S. Jellali, Appl. Water Sci. **9**, 1 (2019)

43. A. Naghizadeh, M. Ghafouri, Iran. J. Chem. Chem. Eng. **36**, 25 (2017)

44. L. Dai, Z. Yao, W. Yang, M. Xia, Y. Ye, Fresenius Environ. Bull. **26**, 4991 (2017)

45. S. Wong, H.H. Tumari, N. Ngadi, N.B. Mohamed, O. Hassan, R. Mat, N. Aishah, S. Amin, J. Clean. Prod. **206**, 394 (2019)

46. A.A. Moosa, A.M. Ridha, N.A. Kadhim, Am. J. Mater. Sci. **6**, 135 (2016)

47. M. Ibrahim, M. Ibrahim, ChemSearch J. **9**, 13 (2018)

48. S.E. Subramani, N. Thinakaran, Process Saf. Environ. Prot. **106**, 1 (2016)

49. G.Z. Kyzas, N. Bikiaris, A.C. Mitropoulos, Polym Int **66**, 1800 (2017)

50. A. El-Imache, K. Ouazzani, Orient. J. Chem. **34**, 2859 (2018)

51. D. Pathania, S. Sharma, P. Singh, Arab. J. Chem. **10**, S1445 (2017)

52. S. Boumchita, A. Lahrichi, Y. Benjelloun, S. Lairini, V. Nenov, F. Zerrouq, J. Mater. Environ. Sci. **8**, 2353 (2017)

53. D. Uzunoğlu, A. Özer, Desalin. Water Treat. **57**, 14109 (2016)

54. S. Fauzia, H. Aziz, D. Dahlan, J. Namieśnik, R. Zein, Desalin. Water Treat. **147**, 191 (2019)

55. X. Guo, Q. Wei, B. Du, Y. Zhang, X. Xin, L. Yan, H. Yu, Appl. Surf. Sci. **284**, 862 (2013)

56. R.K. Gautam, P.K. Gautam, S. Banerjee, V. Rawat, S. Soni, S.K. Sharma, M.C. Chattopadhyaya, J. Environ. Chem. Eng. **3**, 79 (2015)

57. B.O. Isiuku, World News. Nat. Sci. **13**, 10 (2017)

58. L.G. P'yanova, V.A. Likholobov, L.K. Gerunova, M.S. Drozdetskaya, A.V. Sedanova, N.V. Kornienko, Russ. J. Appl. Chem. **90**, 2004 (2017)

59. I. Laurindo, C. Junior, L. Finger, P.P. Quitaiski, S.M. Neitzke, Eclética Química J. **43**, 45 (2018)

60. I. Guerrero-Coronilla, E. Aranda-García, E. Cristiani-Urbina, Environ. Eng. Manag. J. **18**, 1671 (2019)

61. T. Anh, V. Tien, T. Thanh, H. Tran, T. Quynh, N. Le, Morrocan J. Chem. **1**, 18 (2021)